
CHAPTER 8

Modelling type Ia supernova light curves

Bert W. Rust

Mathematical and Computational Sciences Division
National Institute of Standards and Technology (NIST)
100 Bureau Drive, MS 8910
Gaithersburg, MD 20899-8910, USA
bert.rust@nist.gov

Dianne P. O'Leary

Computer Science Department and Institute for Advanced Computer Studies
University of Maryland
College Park, MD 20742; and
National Institute of Standards and Technology
Gaithersburg, MD 20899-8910
oleary@cs.umd.edu

Katharine M. Mullen

Ceramics Division
National Institute of Standards and Technology (NIST)
100 Bureau Drive, M/S 8520
Gaithersburg, MD, 20899, USA
kmullen@nist.gov

ABSTRACT. Type Ia supernova light curves are characterized by a rapid rise from zero luminosity to a peak value, followed by a slower quasi-exponential decline. The rise and peak last for a few days, while the decline persists for many months. It is widely believed that the decline is powered by the radioactive decay chain $^{56}\text{Ni} \rightarrow ^{56}\text{Co} \rightarrow ^{56}\text{Fe}$, but the rates of decline in luminosity do not exactly match the decay rates of Ni and Co. In 1976, Rust, Leventhal, and McCall [19] presented evidence that the declining part of the light curve is well modelled by a linear combination of two exponentials whose decay rates were proportional to, but not exactly equal to, the decay rates for Ni and Co. The proposed reason for the lack of agreement between the rates was that the radioactive decays take place in the interior of a white dwarf star, at densities much higher than any encountered in a terrestrial environment, and that these higher densities accelerate the two decays by the same factor. This paper revisits this model, demonstrating that a variant of it provides excellent fits to observed luminosity data from 6 supernovae.

Keywords: Supernova light curves; exponential modelling; radioactive decays; luminosity data

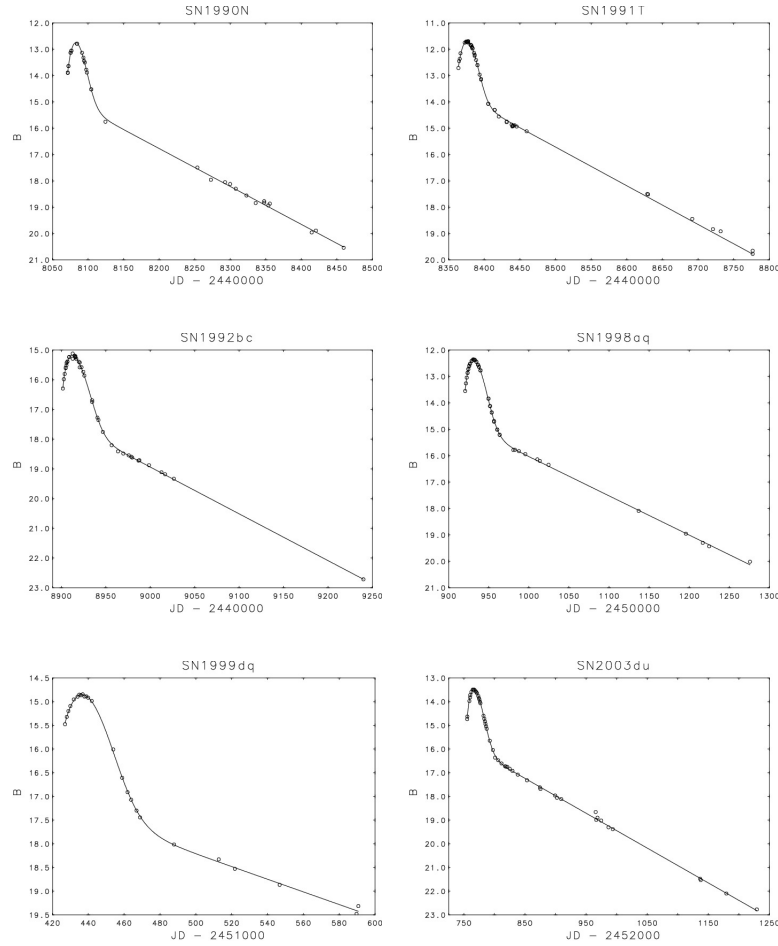


FIGURE 8.1.1. B-magnitude light curves for 6 Type Ia supernovae. The label on each plot is the name assigned to the supernova, specifying the year of the explosion and the order of discovery in that year. The time unit for the measurements is *Julian Days* (JD), the number of days since Greenwich noon on January 1, 4713 BC. The brightness units are astronomical magnitudes measured in the B (blue) wavelength passband.

8.1. Introduction

Supernovae are exploding stars that, for a few weeks, can be as bright as or even brighter than their parent galaxies. Most types of supernovae have irregular light curves, but for one class, Type Ia, the light curves display a very uniform and regular behavior. The light curves of 6 such supernovae are given in Figure 8.1.1, where the discrete data points are measurements of the apparent brightness of the supernova and the smooth curves are fits of a 6-parameter model that will be described in Section 8.2. The similarity of the 6 plots attests to the uniformity of the phenomenon.

This uniformity makes Type Ia supernovae excellent standard candles for estimating distances to their parent galaxies. In 1974 Rust [18, Chapt. 11] demonstrated a linear dependence of estimates of the peak absolute magnitude on the post-maximum rate of decline of the light curve. The absolute magnitude is a measure of the intrinsic luminosity that can be combined with the apparent (observed) magnitude to get an estimate of the distance. If the relationship is calibrated by observations of supernovae in nearby galaxies whose distances can be reliably estimated by other means, then the observed rate of decline of the light curve of a distant supernova leads to an estimate of its absolute magnitude and thence its distance. Rust's sample of light curves was limited and not completely homogeneous, so the linear dependence that he pointed out was scarcely noted by the astronomical community. Fortunately the correlation was rediscovered in 1993 by Phillips [16] who established it as a foundation for Type Ia standard candles. The light curve model that we describe in this paper has potential use in refining this tool for distance estimation.

The uniformity of the linear long time decays in the light curves, together with theoretical considerations, has led to the belief that the light curve is powered by the radioactive decay chain $^{56}\text{Ni} \rightarrow ^{56}\text{Co} \rightarrow ^{56}\text{Fe}$, where the ^{56}Ni is deposited by fusion reactions in a carbon-oxygen white dwarf star [2]. A white dwarf star contains a mass comparable to that of our sun, collapsed into a volume smaller than that of the earth, so the interior densities are extraordinarily high. All atoms in the star are totally stripped of their electrons, which circulate through the interior in a Fermi sea, providing the pressure that keeps the star from collapsing further. The cause of the collapse is thought to be the exhaustion of the hydrogen fuel that provided the fusion energy powering the star before the collapse. According to this theory, the star is part of a binary system in which the other star expands and sheds its outer layers. Some of this lost material falls onto the white dwarf to ignite a new round of fusion reactions that burn the carbon and oxygen to produce ^{56}Ni . One problem for this scenario is the fact that the supernova light curve decay rates are always faster than the terrestrial decay rates of ^{56}Ni and ^{56}Co .

In 1974 Van Hise [22] analyzed the light curve of SN1937c. He found two decay rates, faster than those of (terrestrial) ^{56}Ni and ^{56}Co , but having approximately the same ratio as these rates. Thus the decays in the star seemed to be accelerated by the same factor. In a terrestrial environment, ^{56}Ni beta decays to ^{56}Co entirely by electron capture, and ^{56}Co beta decays to ^{56}Fe by electron capture 80 % of the time. In 1975, Leventhal and McCall [12] suggested that the decays occur in the high-density interior of the white dwarf, where the electron capture rates are enhanced. In 1976, Rust, Leventhal and McCall [19] fit a model consisting of a sum of two exponentials to the post-maximum light curves for 15 supernovae. This work was one of the first real-world applications of the renowned *VARPRO* [5, 6] program for solving separable non-linear least squares problems, and the first of many subsequent applications of the variable projection algorithm in spectroscopy [14]. They found a statistically significant correlation between the two exponential decay rates, with average lifetime values $\tau_1 = (6.46 \pm 1.98) \text{ d}$ and $\tau_2 = (81.2 \pm 25.7) \text{ d}$ ¹. The ratio of these two values, $81.2/6.46 = 12.6$ is approximately the same as the ratio $111.42/8.764 = 12.71$ of the terrestrial average lifetimes of ^{56}Co and

¹The abbreviation "d" denotes "days", and we have specified standard uncertainties for the quantities.

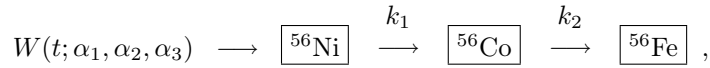
^{56}Ni . In spite of this evidence, the astronomical community [1, 3] rejected the Leventhal and McCall hypothesis, and concluded that even though the light curve is powered by the radioactive decay chain, the observed decay rates were not related to the radioactive decay rates, but rather depended on the physical conditions of the expanding atmosphere of the supernova, and that the apparent exponential decay in the late-time light curve was not even necessarily a true exponential. Placing a straight edge along the long tails in the light curves in Figure 8.1.1 provides a sufficient rebuttal to this last idea.

In this paper we revisit this data-fitting problem, using higher-quality data that have become available since the 1970s. We describe our model in Section 8.2 and the computational tools and results in Sections 8.3 and 8.4. Our basic hypothesis is that radioactive β -decay rates increase in high density environments by an amount proportional to the density. While as far as we know this result is not predicted by theory, other explanations of the apparent observed increase in decay rates are not forthcoming. We show that under this hypothesis, the B-passband light curve is well explained, and that combining those results with a light echo effect allows the luminosity evolution in the other passbands to be explained also.

8.2. The basic model

We present a model consistent with the assumption that the fusion reactions that deposit the ^{56}Ni and the subsequent decays to ^{56}Co and ^{56}Fe all occur in the interior of a white dwarf that is not totally disrupted by the outburst. The atmosphere of the star may be exploded outward, but the central engine powering the whole outburst remains intact, providing a very stable energy source that maintains a constant, enhanced decay rate even at very late times in the light curve. The energy is generated in the form of gamma ray photons that are degraded to visible light by interactions with the expanding atmosphere and possibly also with a pre-existing planetary nebula surrounding the white dwarf.

The model can be represented schematically as follows:



where $W(t; \alpha_1, \alpha_2, \alpha_3)$ is a pulse of ^{56}Ni deposition and k_1 and k_2 are the nuclear decay rates of ^{56}Ni and ^{56}Co . The initial pulse is modelled by a Weibull probability density function

$$W(t; \alpha_1, \alpha_2, \alpha_3) = \frac{\alpha_2}{\alpha_3} \left(\frac{t - \alpha_1}{\alpha_3} \right)^{(\alpha_2 - 1)} \exp \left[- \left(\frac{t - \alpha_1}{\alpha_3} \right)^{\alpha_2} \right] , \quad (8.1)$$

where α_1 is a location parameter, α_2 is a shape parameter, and α_3 is a scale parameter. These three adjustable parameters give the Weibull function great flexibility in modelling the Ni deposition process. Note that the parameter α_1 is the starting time for the fusion pulse.

In a terrestrial setting, the decay rates k_1 and k_2 would be the inverses of the average lifetimes 8.764 d and 111.42 d, but in the high density interior of the star, the model allows these two rates to be accelerated by a common factor α_4 , so

$$k_1 = \frac{1}{8.764 \alpha_4} , \quad k_2 = \frac{1}{111.42 \alpha_4} , \quad (8.2)$$

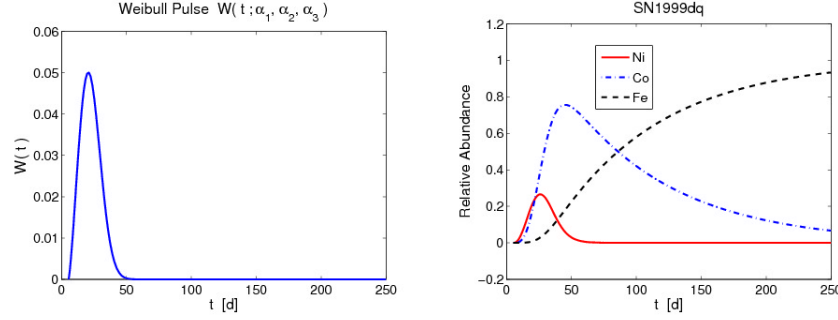


FIGURE 8.2.1. The Weibull pulse for SN1999dq and the relative abundances of Ni, Co and Fe that it generates.

and α_4 becomes a fourth parameter for the model. If $N_1(t)$, $N_2(t)$, and $N_3(t)$ represent the abundances of ^{56}Ni , ^{56}Co , and ^{56}Fe , respectively, then the ordinary differential equations (ODEs) for the ^{56}Ni deposition and subsequent decay processes can be written

$$\begin{aligned} \frac{dN_1}{dt} &= W(t; \alpha_1, \alpha_2, \alpha_3) - \frac{1}{8.764 \alpha_4} N_1, & N_1(\alpha_1) &= 0, \\ \frac{dN_2}{dt} &= \frac{1}{8.764 \alpha_4} N_1 - \frac{1}{111.42 \alpha_4} N_2, & N_2(\alpha_1) &= 0, \\ \frac{dN_3}{dt} &= \frac{1}{111.42 \alpha_4} N_2, & N_3(\alpha_1) &= 0. \end{aligned} \quad (8.3)$$

Since the Weibull pulse is a probability density function, it has unit area, which means that it produces a unit amount of ^{56}Ni , so $N_1(t)$, $N_2(t)$ and $N_3(t)$ are relative abundances that are scaled up in the fit of the model to the observed data. Plots of the Weibull pulse and the relative abundances that it produces for the supernova SN1999dq are given in Figure 8.2.1.

It is luminosity generated by the nuclear decays, rather than relative abundance, that is actually observed. We can write our model for luminosity in the standard *VARPRO* notation by defining

$$\Phi_1(t; \boldsymbol{\alpha}) = \frac{1}{8.764 \alpha_4} N_1(t), \quad \Phi_2(t; \boldsymbol{\alpha}) = \frac{1}{111.42 \alpha_4} N_2(t), \quad (8.4)$$

where Φ_1 and Φ_2 are the relative contributions to the total luminosity by the decays of ^{56}Ni and ^{56}Co , respectively. The total observed luminosity can then be written

$$L(t, \boldsymbol{\alpha}) = C_1 \Phi_1(t; \boldsymbol{\alpha}) + C_2 \Phi_2(t; \boldsymbol{\alpha}), \quad (8.5)$$

where C_1 and C_2 are linear adjustable parameters that convert the relative luminosities to observed luminosities. So our model has 6 free parameters: 4 nonlinear parameters α_1 , α_2 , α_3 , and α_4 that specify the properties of the central engine generating the gamma rays that power the luminosity, and 2 linear parameters C_1 and C_2 that specify how the gamma rays interact with the expanding atmosphere and/or the surrounding planetary nebula to generate the observed luminosity. It is easy to get initial estimates for α_1 and α_4 from the observed light curves. It is somewhat more difficult to get initial estimates of α_2 and α_3 . Since we used *VARPRO* to do the fits, no initial estimates for C_1 and C_2 were needed.

8.3. Fitting the model to the B-passband observations

Substituting Eqs. (8.4) into (8.5) allows us to write the model in the form

$$L(t, \alpha) = C_1 \frac{1}{8.764 \alpha_4} N_1(t) + C_2 \frac{1}{111.42 \alpha_4} N_2(t), \quad (8.6)$$

where $N_1(t)$ and $N_2(t)$ depend on α_1 , α_2 , and α_3 and are obtained by solving the system of ODEs (8.3). It is possible to find closed form solutions for $N_1(t)$ and $N_2(t)$, but the formulas obtained are complicated, involving an integral of the Weibull pulse (8.1). The formulas for the partial derivatives $\partial\Phi_1/\partial\alpha$ and $\partial\Phi_2/\partial\alpha$ are even more complicated, so we instead compute $N_1(t)$ and $N_2(t)$ by numerically integrating the system (8.3) using the Runge-Kutta code DERKF [20].

8.3.1. Choice of units. In the light curves in Figure 8.1.1, astronomical magnitudes are plotted versus Julian Days, but this is not the space in which the fits were computed.

Julian Day would be a very unwieldy time variable, so for each supernova, the zero point for the time t was reset to be a few days before the first observed magnitude. Row 5 in Tables 1 and 2 gives, for each of the 6 supernovae, the Julian Day chosen to define the zero point for t .

Astronomical magnitude would also be an unwieldy variable for fitting. The magnitude scale is logarithmic, with a difference of five magnitudes corresponding to a change by a factor of 100 in apparent brightness. The scale runs backward, with smaller magnitudes corresponding to brighter objects. To produce a more convenient variable for fitting, a reference magnitude B_{ref} was chosen for each supernova, and the measured magnitudes B_i were converted to *relative luminosities* L_i by the formula

$$L_i = 10^{-0.4(B_i - B_{ref})}. \quad (8.7)$$

The reference magnitudes chosen for each of the supernovae are given in row 6 of Tables 1 and 2. So the fits were calculated in the $\{t, L\}$ space, and the light curves obtained were transformed back to the $\{JD, B\}$ space, using the inverse relation

$$B(t) = B_{ref} - 2.5 \log_{10}[L(t)], \quad (8.8)$$

to get the light curves plotted in Figure 8.1.1.

8.3.2. The variational equations for the partial derivatives. The model (8.6) is nonlinear in the four parameters α , so it was necessary for *VARPRO* to iterate in the 4-dimensional α -space. That required the 8 partial derivatives

$$\frac{\partial\Phi_1}{\partial\alpha} = \frac{\partial}{\partial\alpha} \left[\frac{1}{8.764 \alpha_4} N_1(t) \right], \quad \frac{\partial\Phi_2}{\partial\alpha} = \frac{\partial}{\partial\alpha} \left[\frac{1}{111.42 \alpha_4} N_2(t) \right]. \quad (8.9)$$

All attempts to use finite difference approximations to these derivatives met with complete failure. *VARPRO* was never able to improve on any given set of initial estimates when it was using numerical derivatives. The fact that noisy derivatives cause difficulty in optimization settings has been previously documented; see, e.g., [11].

Analytic derivatives can be obtained by noting that

$$\frac{\partial \Phi_1}{\partial \alpha_j} = \frac{1}{8.764 \alpha_4} \frac{\partial N_1}{\partial \alpha_j}, \quad j = 1, 2, 3, \quad (8.10)$$

$$\frac{\partial \Phi_1}{\partial \alpha_4} = \frac{1}{8.764 \alpha_4} \frac{\partial N_1}{\partial \alpha_4} - \frac{1}{8.764 \alpha_4^2} N_1, \quad (8.11)$$

$$\frac{\partial \Phi_2}{\partial \alpha_j} = \frac{1}{111.42 \alpha_4} \frac{\partial N_2}{\partial \alpha_j}, \quad j = 1, 2, 3, \quad (8.12)$$

$$\frac{\partial \Phi_2}{\partial \alpha_4} = \frac{1}{111.42 \alpha_4} \frac{\partial N_2}{\partial \alpha_4} - \frac{1}{111.42 \alpha_4^2} N_2. \quad (8.13)$$

Thus the problem is reduced to one of computing the 8 partial derivatives

$$\frac{\partial N_1}{\partial \alpha} \quad \text{and} \quad \frac{\partial N_2}{\partial \alpha},$$

where N_1 and N_2 are defined by the ODEs (8.3). Since we did not want to solve that system in closed form, we instead used the identities

$$\frac{d}{dt} \left(\frac{\partial N_1}{\partial \alpha_j} \right) = \frac{\partial}{\partial \alpha_j} \left(\frac{dN_1}{dt} \right), \quad j = 1, 2, 3, 4, \quad (8.14)$$

$$\frac{d}{dt} \left(\frac{\partial N_2}{\partial \alpha_j} \right) = \frac{\partial}{\partial \alpha_j} \left(\frac{dN_2}{dt} \right), \quad j = 1, 2, 3, 4, \quad (8.15)$$

to extend the system to include 8 more ODEs defining the required partial derivatives. Substituting the derivative expressions from (8.3) into the two expressions above gives

$$\frac{d}{dt} \left(\frac{\partial N_1}{\partial \alpha_j} \right) = \frac{\partial}{\partial \alpha_j} W(t; \alpha_1, \alpha_2, \alpha_3) - \frac{1}{8.764 \alpha_4} \left(\frac{\partial N_1}{\partial \alpha_j} \right), \quad j = 1, 2, 3, \quad (8.16)$$

$$\frac{d}{dt} \left(\frac{\partial N_1}{\partial \alpha_4} \right) = \frac{1}{8.764 \alpha_4^2} N_1 - \frac{1}{8.764 \alpha_4} \left(\frac{\partial N_1}{\partial \alpha_4} \right), \quad (8.17)$$

$$\frac{d}{dt} \left(\frac{\partial N_2}{\partial \alpha_j} \right) = \frac{1}{8.764 \alpha_4} \left(\frac{\partial N_1}{\partial \alpha_j} \right) - \frac{1}{111.42 \alpha_4} \left(\frac{\partial N_2}{\partial \alpha_j} \right), \quad j = 1, 2, 3, \quad (8.18)$$

$$\begin{aligned} \frac{d}{dt} \left(\frac{\partial N_2}{\partial \alpha_4} \right) = & -\frac{1}{8.764 \alpha_4^2} N_1 + \frac{1}{111.42 \alpha_4^2} N_2 \\ & + \frac{1}{8.764 \alpha_4} \left(\frac{\partial N_1}{\partial \alpha_4} \right) - \frac{1}{111.42 \alpha_4} \left(\frac{\partial N_2}{\partial \alpha_4} \right), \end{aligned} \quad (8.19)$$

which, using the initial conditions

$$\frac{\partial N_1}{\partial \alpha_j} = 0, \quad \frac{\partial N_2}{\partial \alpha_j} = 0, \quad j = 1, 2, 3, 4, \quad (8.20)$$

can be integrated numerically along with the ODEs in (8.3). But to do so, it is necessary to find expressions for the 3 partial derivatives of $W(t; \alpha_1, \alpha_2, \alpha_3)$ defined by (8.1). We used Matlab's *Symbolic Math Toolbox* with the program

```

syms a1 a2 a3 t

w = a2/a3*(t-a1)^(a2-1)/a3^(a2-1) * exp(-((t-a1)/a3)^a2)

dw_da1 = diff(w,a1)
dw_da2 = diff(w,a2)
dw_da3 = diff(w,a3)

fortran(dw_da1)
fortran(dw_da2)
fortran(dw_da3)

```

to generate not only the symbolic derivatives, but also Fortran statements to be inserted into a Fortran subroutine for computing them numerically.

8.3.3. The fits. We fit the model (8.6) to the relative luminosity data for the 6 supernovae whose relative luminosity light curves are plotted in Figure 8.3.1. These particular 6 examples were chosen for this study because they have modern photometric observations, in several wavelength passbands, with observations beginning well before maximum luminosity, and with B-passband light curve data extending at least 150 days past that maximum. The shortest light curve (SN1999dq) contains 25 data points spanning 163.66 days, and the longest (SN2003du) contains 51 data points spanning 474.04 days.

In computing the fits, we weighted each observation inversely with the observed luminosity so that all of the observations contributed equally to determining the parameter estimates. This was absolutely necessary to assure that the long tails were fitted as well as the peaks. The good fits in the tails in Figure 8.1.1 demonstrate the effectiveness of this weighting strategy. Even very small misfits in the tails in Figure 8.3.1 would have transformed into large misfits in the tails in Figure 8.1.1.

We have already noted that *VARPRO* was unable to improve on our initial estimates when we used numerical approximations for the partial derivatives (8.9). Programming the analytic derivatives by the method outlined in Section 8.3.2 was an intricate and complicated task, but using them enabled *VARPRO* to always converge to a good fit, even if the initial estimates were poor. However, a surprisingly large number of iterations was required for convergence. If the initial estimates were not very close to the final converged values, then 20 000 - 40 000 iterations might be required. Apparently this simple model produces a very difficult fitting problem, even though we were iterating in a 4-dimensional space rather than the 6-dimensional space required by conventional nonlinear least squares programs that do not take advantage of the conditional linearity of C_1 and C_2 .

We checked to see if any of the observed luminosity could have come from the fusion reactions in the Weibull pulse. We did this by appending an additional term

$$C_3\Phi_3(t; \alpha) = C_3W(t; \alpha_1, \alpha_2, \alpha_3) \quad (8.21)$$

to the model and fitting it to several light curves. In every case the modified model failed to yield a significant improvement in the fit. The fits often gave physically meaningless estimates for C_3 , e.g., $\hat{C}_3 = -15 \pm 124$ for SN1992bc, and always gave covariance matrices exhibiting extremely high correlations, e.g., $\pm 0.999 \dots$ between

some of the parameters. This is a sure indication of a model with too many free

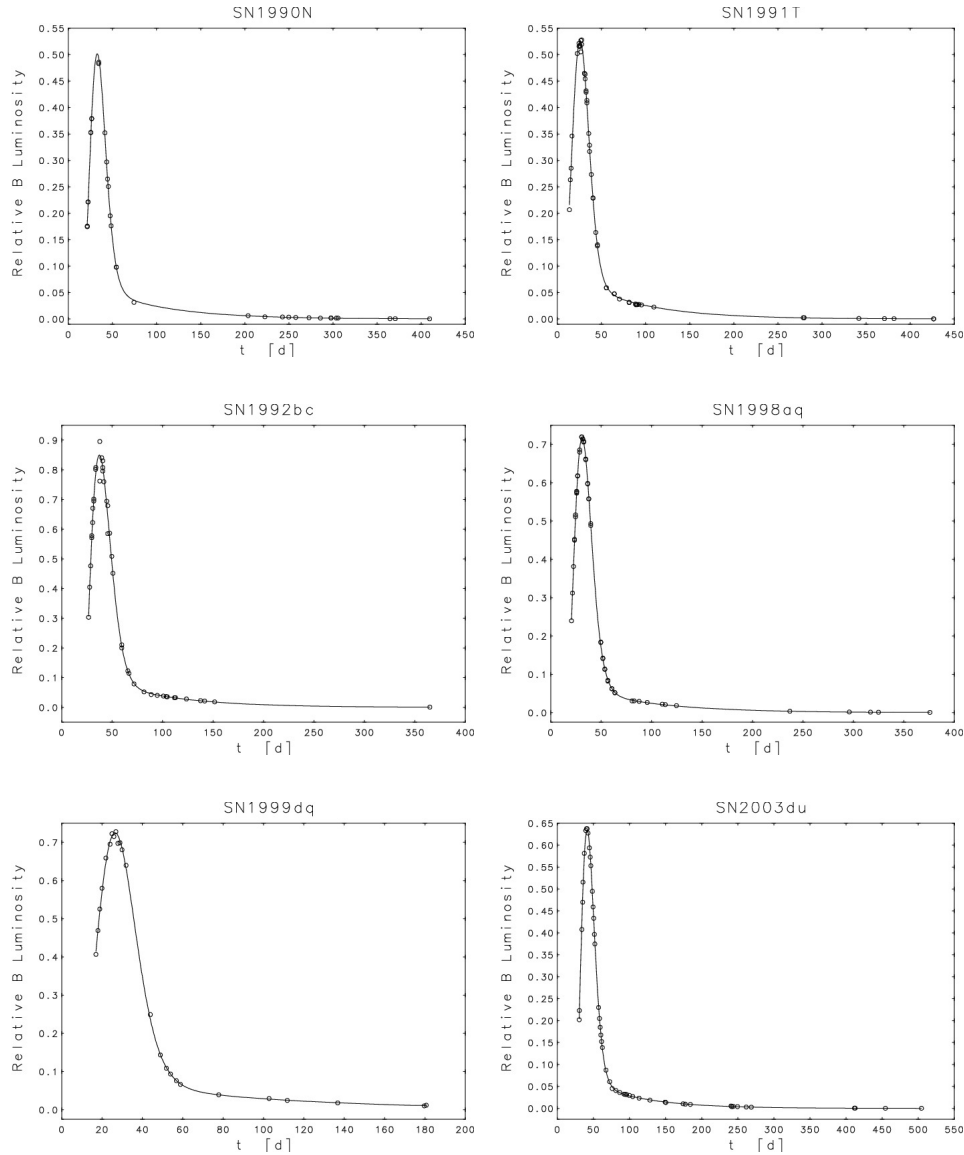


FIGURE 8.3.1. B-luminosity light curves for the 6 supernovae whose B-magnitude light curves are plotted in Figure 8.1.1. The observed luminosities here were computed by applying the transform (8.7) to the observed magnitudes plotted in Figure 8.1.1. The curves shown here were obtained by fitting the model (8.6) to these observed luminosities. The curves shown in Figure 8.1.1 were calculated by applying the inverse transform (8.8) to the curves shown here.

parameters. Thus it appears that all of the observed luminosity from a Type Ia supernova comes from the radioactive decay chain.

The parameter estimates and their uncertainties for the 6 supernovae are given, together with some other pertinent data, in Tables 1 and 2. The key to these tables follows:

- row 1:** Source for the measured magnitudes.
- row 2:** Name of the parent galaxy.
- row 3:** Galactocentric velocity of recession implied by measured redshift of the galaxy. These data, together with those in row 4, were taken from the NASA/IPAC Extragalactic Database (NED) [10] which is operated by JPL under contract with NASA.
- row 4:** Galactocentric distance to the galaxy estimated from the Hubble law $V_r = H_0 D$ using $H_0 = (73.0 \pm 5.0)$ km/s/Mpc, where the units are kilometers per second per 10^6 parsecs.
- row 5:** Julian Day chosen for zero point in time.
- row 6:** Reference magnitude used in Eqs. (8.7) and (8.8) for transforming between magnitudes and relative luminosities.
- row 7:** Estimate of Weibull location parameter (gives time of initial eruption of Weibull pulse).
- row 8:** Estimate of Weibull shape parameter.
- row 9:** Estimate of Weibull scale parameter.
- row 10:** Estimate of acceleration parameter speeding up Ni and Co decay rates.
- row 11:** Estimate of linear parameter which determines how supernova's atmosphere transforms energy from Ni decays into observed luminosity.
- row 12:** Estimate of linear parameter which determines how supernova's atmosphere transforms energy from the Co decays into observed luminosity.
- row 13:** Percentage of total variance explained by fit. R^2 is from Eq. (8.22).
- row 14:** Time of maximum luminosity.
- row 15:** Julian Day of maximum luminosity.
- row 16:** B magnitude at maximum luminosity.

Since the fits were nonlinear, the uncertainties for the parameter estimates were derived from an estimate of the covariance matrix based on a local quadratic approximation to the sum-of-squared-residuals (SSR) surface at the point where the SSR was minimized. Therefore those uncertainties should be treated with caution. The value R^2 in row 13 of the table is the coefficient of determination,

$$R^2 = 1 - \frac{SSR}{CTSS}, \quad (8.22)$$

where SSR is the weighted residual sum of squares and $CTSS$ is the corrected total sum of squares. The latter quantity is computed by

$$CTSS = \sum_{i=1}^N w_i^2 (L_i - \bar{L})^2, \quad (8.23)$$

where the L_i , $i = 1, \dots, N$, are the observed relative luminosities, \bar{L} is the weighted average luminosity, and the $w_i = 1/L_i$ are the weights used in the fits. Thus R^2 is a normalized residual sum of squares which will always have a value between 0 and 1. We express it as a percentage, indicating the percentage of the total variance.

TABLE 1. Results for SN1990N, SN1991T, and SN1992bc for the B passband.

	SN	1990N	1991T	1992bc
1	Reference	[13]	[13]	[8]
2	Galaxy	NGC 4639	NGC 4527	ESO 300-9
3	V_r [km/s]	974 ± 6	1654 ± 3	5881 ± 600
4	D [Mpc]	13.3 ± 0.9	22.7 ± 1.6	80.6 ± 10.0
5	JD ($t = 0$)	2 448 050.0	2 448 350.0	2 448 875.0
6	B_{ref}	12.0	11.0	15.0
7	$\hat{\alpha}_1$	13.7 ± 1.6	2.1 ± 2.8	$22.08 \pm .40$
8	$\hat{\alpha}_2$	$2.32 \pm .25$	$2.66 \pm .34$	$1.730 \pm .052$
9	$\hat{\alpha}_3$	17.5 ± 1.6	22.0 ± 2.9	$15.56 \pm .43$
10	$\hat{\alpha}_4$	$0.676\,078\,5$ $\pm .000\,006\,8$	$0.662\,474\,7$ $\pm .000\,003\,0$	$0.618\,920\,3$ $\pm .000\,004\,3$
11	\hat{C}_1	$10.63 \pm .22$	$12.02 \pm .16$	$19.21 \pm .17$
12	\hat{C}_2	$4.24 \pm .10$	$5.004 \pm .080$	$6.104 \pm .073$
13	R^2	99.57 %	99.67 %	99.88 %
14	t_{\max} [d]	32.83	25.91	37.36
15	JD_{\max}	2 448 082.83	2 448 375.91	2 448 912.36
16	B_{\max}	12.75	11.70	15.18

8.4. Extending the model to U-, V-, R- and I-passband observations

The B passband light curves in Figures 8.1.1 and 8.3.1 are quite extraordinary. But the model is not so successful when it is fit to observations in other wavelength passbands. Astronomers often measure apparent brightness in 5 different passbands, U, B, V, R, and I which represent ultraviolet, blue, visual, red, and infrared, respectively. The U, B, V, R, and I light curves for SN2003du are shown in Figure 8.4.1. The departures of the measurements from the simple model used to fit the B light curve (upper right hand plot) are apparent in the V, R, and I light curves.

8.4.1. A light echo model for the I-passband observations. The most striking departures are in the I light curve, where it appears that a secondary peak occurs about 30 days after the maximum luminosity. This suggests that it may have been caused by a light echo from the back side of a pre-existing shell of dust surrounding the supernova. White dwarfs are often surrounded by planetary nebula which were presumably formed when the parent star ejected its outer layers before

TABLE 2. Results for SN1998aq, SN1999dq, and SN2003du for the B passband.

	SN	1998aq	1999dq	2003du
1	Reference	[17]	[9]	[21]
2	Galaxy	NGC 3982	NGC 976	UGC 9391
3	V_r [km/s]	1187 ± 7	4370 ± 6	2055 ± 7
4	D [Mpc]	16.3 ± 1.1	59.9 ± 4.2	28.1 ± 2
5	JD ($t = 0$)	2 450 900.0	2 451 410.0	2 452 725.0
6	B_{ref}	12.0	14.5	13.0
7	$\hat{\alpha}_1$	$14.72 \pm .40$	5.4 ± 2.6	$25.07 \pm .60$
8	$\hat{\alpha}_2$	$2.085 \pm .058$	$2.37 \pm .29$	$1.966 \pm .095$
9	$\hat{\alpha}_3$	$15.33 \pm .42$	19.3 ± 2.6	$15.40 \pm .66$
10	$\hat{\alpha}_4$	$0.655\,925\,3$ $\pm .000\,003\,1$	$0.729\,83$ $\pm .000\,11$	$0.662\,263\,8$ $\pm .00000\,11$
11	\hat{C}_1	$14.752 \pm .090$	$16.76 \pm .37$	$13.54 \pm .14$
12	\hat{C}_2	$4.355 \pm .043$	$5.59 \pm .18$	$4.395 \pm .048$
13	R^2	99.93 %	99.87 %	99.79 %
14	t_{\max} [d]	31.19	26.45	41.35
15	JD_{\max}	2 450 931.19	2 451 436.45	2 452 766.35
16	B_{\max}	12.36	14.85	13.49

collapsing into a white dwarf. If we make the crude assumption that the echo comes almost entirely from material very close to our line of sight to the star, then we can approximate the observed relative luminosity with a model of the form

$$L(t; \boldsymbol{\beta}) = D_1 \Psi_1(t) + D_2 \Psi_2(t) + D_3 \Psi_3(t; \boldsymbol{\beta}) + D_4 \Psi_4(t; \boldsymbol{\beta}) , \quad (8.24)$$

where the D_i are linear parameters to be determined by fitting, and the functions $\Psi_i(t; \boldsymbol{\beta})$ are defined by

$$\Psi_1(t) = \frac{1}{8.764 \hat{\alpha}_4} \hat{N}_1(t) , \quad (8.25)$$

$$\Psi_2(t) = \frac{1}{111.42 \hat{\alpha}_4} \hat{N}_2(t) , \quad (8.26)$$

$$\Psi_3(t; \boldsymbol{\beta}) = \begin{cases} 0 , & t \leq \hat{\alpha}_1 + \beta_1 \\ \left[\frac{1}{8.764 \hat{\alpha}_4} \hat{N}_1(t - \beta_1) \right] Q(t; \beta_2, \beta_3) , & t > \hat{\alpha}_1 + \beta_1 \end{cases} , \quad (8.27)$$

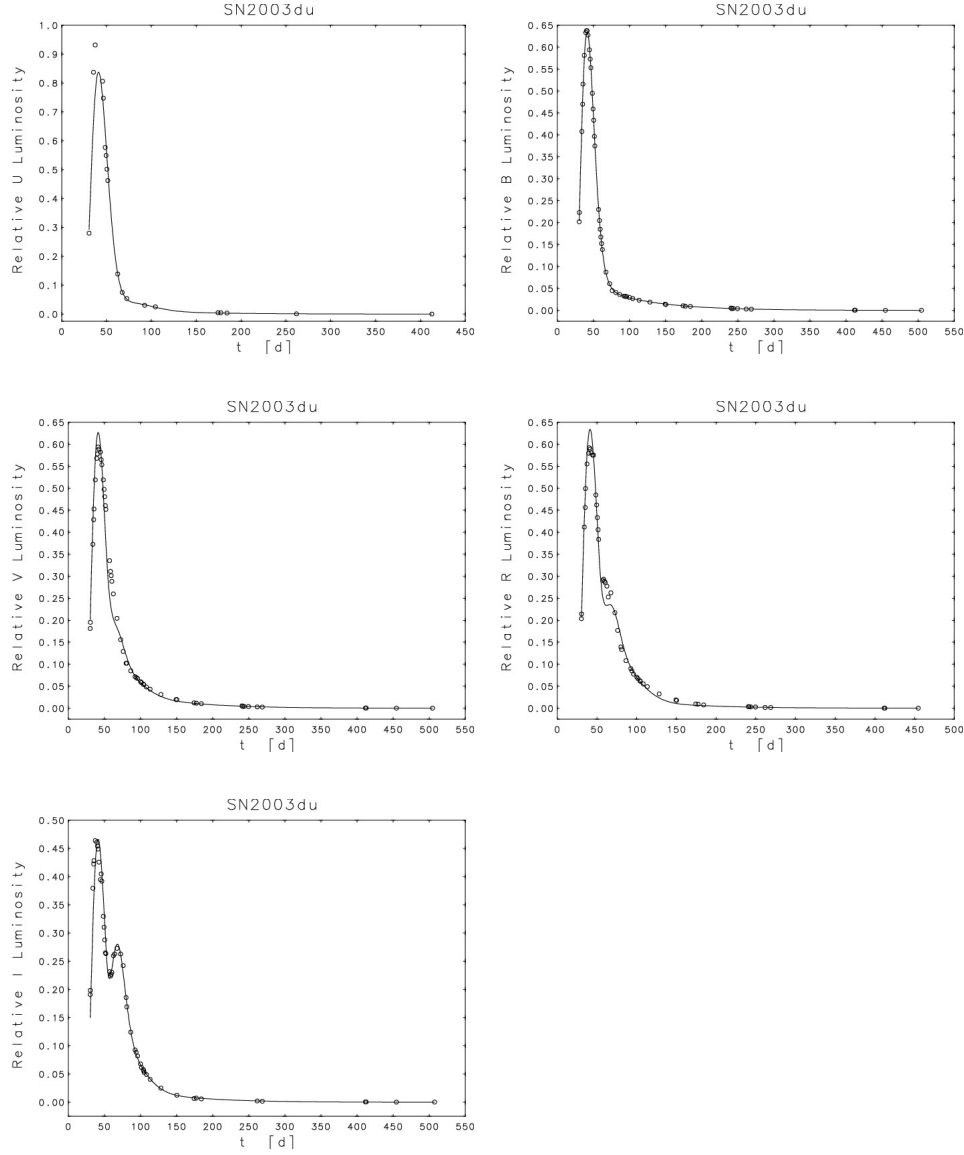


FIGURE 8.4.1. UBVRI light curves, in relative luminosity space, for SN2003du. The discrete points represent the measurements and the smooth curves are model fits. The fit for the B passband is the same as the one in Figure 8.3.1. The other fits are for the model described in section 8.4.

$$\Psi_4(t; \beta) = \begin{cases} 0, & t \leq \hat{\alpha}_1 + \beta_1 \\ \left[\frac{1}{111.42 \hat{\alpha}_4} \hat{N}_2(t - \beta_1) \right] Q(t; \beta_2, \beta_3), & t > \hat{\alpha}_1 + \beta_1 \end{cases}. \quad (8.28)$$

In Eqs. (8.25) and (8.26) the $\hat{\alpha}_4$ is not a parameter to be determined by fitting, but rather the estimate of α_4 that was obtained in fitting the B light curve. Similarly,

the functions $\hat{N}_1(t)$ and $\hat{N}_2(t)$ are the estimates of $N_1(t)$ and $N_2(t)$ that were obtained in the B-curve fit. They depend only on the estimates $\hat{\alpha}$ and do not involve any free parameters to be determined by the fit. The functions $\Psi_3(t; \beta)$ and $\Psi_4(t; \beta)$ are essentially lagged versions of $\hat{N}_1(t)$ and $\hat{N}_2(t)$, with the nonlinear free parameter β_1 being the lag. They are multiplied by a quenching function

$$Q(t; \beta_2, \beta_3) = \frac{1}{2} \operatorname{erfc}[\beta_3(t - \beta_2)], \quad (8.29)$$

which is included to model the vaporization of the reflecting dust as the shell surrounding the supernova is heated to ever higher temperatures. When all of the dust is vaporized, the shell will cease to reflect. We used the complementary error function

$$\operatorname{erfc}(z) = 1 - \operatorname{erf}(z) = 1 - \frac{2}{\sqrt{\pi}} \int_{-\infty}^z \exp(-u^2) du \quad (8.30)$$

to model the quenching because it has the appropriate general shape, and the two free parameters β_2 and β_3 give it the flexibility to model a wide range of possible shapes and extents. The quenching function for SN2003du is shown in Figure 8.4.2.

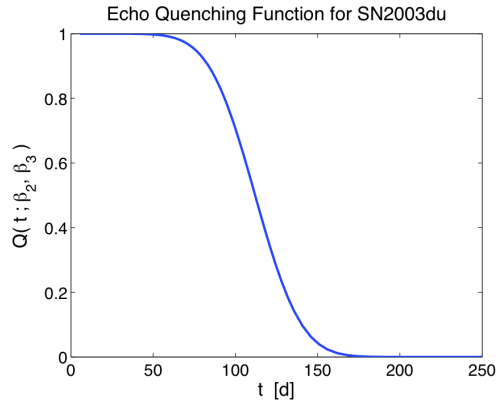


FIGURE 8.4.2. The light echo quenching function for SN2003du

The model (8.24) has 4 linear and 3 nonlinear parameters, which again makes it a candidate for *VARPRO*. It was stable enough to permit the use of numerical derivatives. The fitted I-luminosity light curve for SN2003du is shown in the lower left panel in Figure 8.4.1, and the corresponding parameter estimates are given in column 4 of Table 3. The fit is good, but not as close as the B passband fit. This deterioration in quality is also reflected in the decrease in the R^2 value. The I-magnitude light curve is shown in the lower left panel of Figure 8.4.3. It too is not nearly so close as the B-magnitude light curve in the upper right panel. The decline in the quality of the fit is probably due to the use of a very crude model for the light echo. A proper model would take the spherical geometry of the shell into account, and the light observed at any give time would be a mixture of many different lags. If our light curve model is correct, then the estimate $\hat{\beta}_1 = 27.86$ implies that the inner radius of the reflecting shell is 13.93 light days.

8.4.2. Extending the light echo model to the V, R, and I observations.

Since the I-light curve gave by far the best representation of the light echo, we decided to keep the estimates $\hat{\beta}_1$, $\hat{\beta}_2$, and $\hat{\beta}_3$ fixed in fitting the model to the R, V,

TABLE 3. The parameter estimates for the B, I, R, V, and U light curve fits for SN2003du. The ordering of the columns reflects the order in which the fits were done. A \leftarrow entry means that the value was not a free parameter but rather an estimate obtained in a preceding fit. A blank entry means that neither the corresponding parameter nor its estimate was used in the fit. Row 14 gives the percentage of the total variance explained by the fit, and Row 15 gives the total number of free parameters in the fit.

	Color	B	I	R	V	U
1	$\hat{\alpha}_1$	$25.07 \pm .60$	\leftarrow	\leftarrow	\leftarrow	\leftarrow
2	$\hat{\alpha}_2$	$1.966 \pm .095$	\leftarrow	\leftarrow	\leftarrow	\leftarrow
3	$\hat{\alpha}_3$	$15.40 \pm .66$	\leftarrow	\leftarrow	\leftarrow	\leftarrow
4	$\hat{\alpha}_4$	$0.6622638 \pm .0000011$	\leftarrow	\leftarrow	\leftarrow	\leftarrow
5	\hat{C}_1	$13.54 \pm .14$				
6	\hat{C}_2	$4.395 \pm .048$				
7	$\hat{\beta}_1$		$27.86 \pm .90$	\leftarrow	\leftarrow	\leftarrow
8	$\hat{\beta}_2$		112 ± 34	\leftarrow	\leftarrow	\leftarrow
9	$\hat{\beta}_3$		$0.032 \pm .029$	\leftarrow	\leftarrow	\leftarrow
10	\hat{D}_1		$9.95 \pm .42$	$13.72 \pm .57$	$13.34 \pm .38$	18.37 ± 0.94
11	\hat{D}_2		$3.34 \pm .21$	$2.81 \pm .14$	$4.75 \pm .15$	$1.54 \pm .11$
12	\hat{D}_3		$4.38 \pm .58$	$3.07 \pm .43$	$1.80 \pm .25$	$-0.12 \pm .19$
13	\hat{D}_4		6.2 ± 7.1	$7.52 \pm .66$	$3.97 \pm .41$	$2.59 \pm .48$
14	R^2	99.79 %	97.32 %	96.94 %	98.55 %	97.95 %
15	N_{fp}	6	7	4	4	4

and U light curves. This means that each of those fits was a linear least squares problem with only 4 free parameters. The results, shown in Figures 8.4.1 and 8.4.3, are reasonably good fits. It is not obvious why the light echo would appear in the U but not in the B observations. Perhaps the departures from regularity in the U light curve are due to limb brightening rather than a light echo.

Row 15 of Table 3 gives the number of free parameters in each fit. It is remarkable that we were able to get good fits to five different light curves using an average of only 5 free parameters per fit.

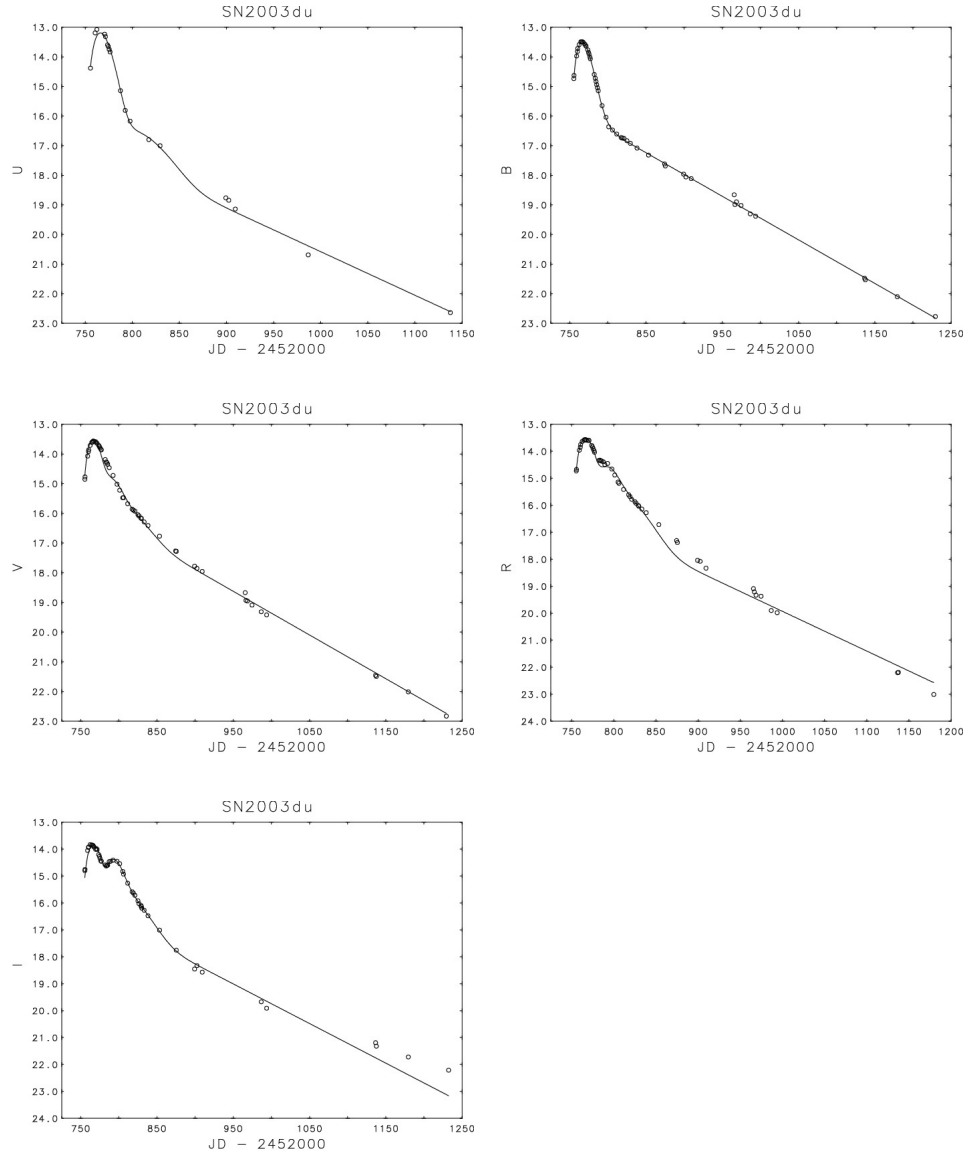


FIGURE 8.4.3. UBVR magnitude light curves for SN2003du, calculated by applying the inverse transform (8.8) to the relative luminosity curves in Figure 8.4.1.

8.5. Conclusion

We have proposed a model for Type Ia supernova light curves and validated it using observed luminosity data from 6 supernovae. Our results support the hypothesis that decay rates for Ni and Co are proportional to, but not exactly equal to, their terrestrial values, perhaps because higher densities accelerate the two decays by the same factor.

Our model was fit using the *VARPRO* algorithm. *VARPRO*'s reduction of the parameter space is essential for the efficiency and even the feasibility of studying such models.

In future work we will examine differences in transmission curves as a source of error in comparing fits from one supernovae to another, and we will compare the UVRI fits for these supernovae. We will also investigate the idea of fitting multiple passbands simultaneously; see, for example, [4, 7, 14].

Acknowledgments

The authors would like to thank Drs. David Gilsinn, Stefan Leigh, and Daniel Lozier for their advice and encouragement. The light curve data were found using two very helpful websites [10, 15].

Disclaimer

Certain commercial software products are identified in this paper in order to adequately specify the computational procedures. Such identification does not imply recommendation or endorsement by the National Institute of Standards and Technology nor does it imply that the software products are necessarily the best available for the purpose.

Bibliography

1. R. Barbon, E. Cappellaro, and M. Turatto, *Radioactive decays and supernova light curves*, *Astronomy and Astrophysics* **135** (1984), 27–31.
2. D. Branch and G. A. Tammann, *Type IA supernovae as standard candles*, *Annual Reviews of Astronomy and Astrophysics* **30** (1992), 359–389.
3. S. A. Colgate, A. G. Petschek, and J. T. Kriese, *The luminosity of type I supernovae*, *Astrophysical Journal Letters* **237** (1980), L81–L85.
4. D. Gay and L. Kaufman, *Tradeoffs in algorithms for separable and block separable nonlinear least squares*, IMACS '91, Proceedings of the 13th World Congress on Computational and Applied Mathematics (Dublin) (R. Vichnevetsky and J. J. H. Miller, eds.), Criterion Press, 1991, pp. 157–158.
5. G. H. Golub and V. Pereyra, *The differentiation of pseudo-inverses and nonlinear least squares problems whose variables separate*, Tech. report, Stanford University, Department of Computer Science, 1972.
6. G. H. Golub and V. Pereyra, *The differentiation of pseudoinverses and nonlinear least squares problems whose variables separate*, *SIAM Journal on Numerical Analysis* **10** (1973), 413–432.
7. G. H. Golub and R. J. LeVeque, *Extensions and uses of the variable projection algorithm for solving nonlinear least squares problems*, Proceedings of the 1979 Army Numerical Analysis and Computers Conference, 1979, pp. 1–12.
8. M. Hamuy, M. M. Phillips, N. B. Suntzeff, R. A. Schommer, J. Maza, A. R. Antezan, M. Wischnjewsky, G. Valladares, C. Muena, L. E. Gonzales, R. Aviles, L. A. Wells, R. C. Smith, M. Navarrete, R. Covarrubias, G. M. Williger, A. R. Walker, A. C. Layden, J. H. Elias, J. A. Baldwin, M. Hernandez, H. Tirado, P. Ugarte, R. Elston, N. Saavedra, F. Barrientos, E. Costa, P. Lira, M. T. Ruiz, C. Anguita, X. Gomez, P. Ortiz, M. della Valle, J. Danziger, J. Storm, Y.-C. Kim, C. Bailyn, E. P. Rubenstein, D. Tucker, S. Cersosimo, R. A. Mendez, L. Siciliano, W. Sherry, B. Chaboyer, R. A. Koopmann, D. Geisler, A. Sarajedini, A. Dey, N. Tyson, R. M. Rich, R. Gal, R. Lamontagne, N. Caldwell, P. Guhathakurta, A. C. Phillips, P. Szkody, C. Prosser, L. C. Ho, R. McMahan, G. Baggley, K.-P. Cheng, R. Havlen, K. Wakamatsu, K. Janes, M. Malkan, F. Baganoff, P. Seitzer, M. Shara, C. Sturch, J. Hesser, A. N. P. Hartig, J. Hughes, D. Welch, T. B. Williams, H. Ferguson, P. J. Francis, L. French, M. Bolte, J. Roth, S. Odewahn, S. Howell, and W. Krzeminski, *BVRI light curves for 29 type IA supernovae*, *Astronomical Journal* **112** (1996), 2408–2437.
9. S. Jha, R. P. Kirshner, P. Challis, P. M. Garnavich, T. Matheson, A. M. Soderberg, G. J. M. Graves, M. Hicken, J. F. Alves, H. G. Arce, Z. Balog, P. Barmby, E. J. Barton, P. Berlind, A. E. Bragg, C. Briceño, W. R. Brown, J. H. Buckley, N. Caldwell, M. L. Calkins, B. J. Carter, K. D. Concannon, R. H. Donnelly, K. A. Eriksen, D. G. Fabricant, E. E. Falco, F. Fiore, M. R. Garcia, M. Gómez, N. A. Grogin, T. Groner, P. J. Groot, K. E. Haisch, Jr., L. Hartmann, C. W. Hergenrother, M. J. Holman, J. P. Huchra, R. Jayawardhana, D. Jerius, S. J. Kannappan, D.-W. Kim, J. T. Kleyna, C. S. Kochanek, D. M. Koranyi, M. Krockenberger, C. J. Lada, K. L. Luhman, J. X. Luu, L. M. Macri, J. A. Mader, A. Mahdavi, M. Marengo, B. G. Marsden, B. A. McLeod, B. R. McNamara, S. T. Megeath, D. Moraru, A. E. Mossman, A. A. Muench, J. A. Muñoz, J. Muzerolle, O. Naranjo, K. Nelson-Patel, M. A. Pahre, B. M. Patten, J. Peters, W. Peters, J. C. Raymond, K. Rines, R. E. Schild, G. J. Sobczak, T. B. Spahr, J. R. Stauffer, R. P. Stefanik, A. H. Szentgyorgyi, E. V. Tollestrup, P. Väisänen, A. Vikhlinin, Z. Wang, S. P. Willner, S. J. Wolk, J. M. Zajac, P. Zhao, and K. Z. Stanek, *UBVRI light curves of 44 type Ia supernovae*, *Astronomical Journal* **131** (2006), 527–554.
10. J. P. Laboratory, *NASA/IPAC extragalactic database (NED)*, <http://nedwww.ipac.caltech.edu/>, accessed June 2009.

11. R. Leidenberger and K. Urban, *Automatic differentiation for the optimization of a ship propulsion and steering system*, Tech. report, University of Ulm, Germany, 2008.
12. M. Leventhal and S. L. McCall, *Hypothesis for the type I supernova light curve*, *Nature* **255** (1975), 690–692.
13. P. Lira, N. B. Suntzeff, M. M. Phillips, M. Hamuy, J. Maza, R. A. Schommer, R. C. Smith, L. A. Wells, R. Avilés, J. A. Baldwin, J. H. Elias, L. González, A. Layden, M. Navarrete, P. Ugarte, A. R. Walker, G. M. Williger, F. K. Baganoff, A. P. S. Crotts, R. M. Rich, N. D. Tyson, A. Dey, P. Guhathakurta, J. Hibbard, Y.-C. Kim, D. M. Rehner, E. Siciliano, J. Roth, P. Seitzer, and T. B. Williams, *Optical light curves of the Type IA supernovae SN 1990N and 1991T*, *Astronomical Journal* **115** (1998), 234–246.
14. K. M. Mullen and I. H. M. van Stokkum, *The variable projection algorithm in time-resolved spectroscopy, microscopy and mass spectrometry applications*, *Numerical Algorithms* **51** (2009), 1017–1398.
15. N. Pavlyuk and the SAI Supernovae Research Group, *SAI supernova light curve online*, <http://virtual.sai.msu.ru/~pavlyuk/snlcurve/>, accessed June 2009.
16. M. M. Phillips, *The absolute magnitudes of Type IA supernovae*, *Astrophysical Journal Letters* **413** (1993), L105–L108.
17. A. G. Riess, W. Li, P. B. Stetson, A. V. Filippenko, S. Jha, R. P. Kirshner, P. M. Challis, P. M. Garnavich, and R. Chornock, *Cepheid calibrations from the Hubble space telescope of the luminosity of two recent type Ia supernovae and a redetermination of the Hubble constant*, *Astrophysical Journal* **627** (2005), 579–607.
18. B. W. Rust, *Use of Supernovae Light Curves for Testing the Expansion Hypothesis and Other Cosmological Relations*, Univ. of Illinois, ORNL-4953, Ph.D. thesis, Oak Ridge National Lab., TN., December 1974.
19. B. W. Rust, M. Leventhal, and S. L. McCall, *Evidence for a radioactive decay hypothesis for supernova luminosity*, *Nature* **262** (1976), 118–120.
20. L. F. Shampine and H. A. Watts, *DEPAC – design of a user oriented package of ODE solvers*, Tech. Report SAND79-2374, Sandia National Laboratories, Albuquerque, NM, September 1980.
21. V. Stanishev, A. Goobar, S. Benetti, R. Kotak, G. Pignata, H. Navasardyan, P. Mazzali, R. Amanullah, G. Garavini, S. Nobili, Y. Qiu, N. Elias-Rosa, P. Ruiz-Lapuente, J. Mendez, P. Meikle, F. Patat, A. Pastorello, G. Altavilla, M. Gustafsson, A. Harutyunyan, T. Iijima, P. Jakobsson, M. V. Kichizhieva, P. Lundqvist, S. Mattila, J. Melinder, E. P. Pavlenko, N. N. Pavlyuk, J. Sollerman, D. Y. Tsvetkov, M. Turatto, and W. Hillebrandt, *SN 2003du: 480 days in the life of a normal type Ia supernova*, *Astronomy and Astrophysics* **469** (2007), 645–661.
22. J. R. van Hise, *Light-decay curve of the supernova in IC 4182*, *Astrophysical Journal* **192** (1974), 657–659.